Spin-$\frac{1}{2}$ J_1-J_2 model on the body-centered cubic lattice

R. Schmidt,* J. Schulenburg, and J. Richter
Institut für Theoretische Physik, Universität Magdeburg, P.O. Box 4120, D-39016 Magdeburg, Germany

D. D. Betts
Department of Physics, Dalhousie University, Halifax, Nova Scotia, Canada B3H 3J5

(Received 4 March 2002; revised manuscript received 29 August 2002; published 11 December 2002)

Using exact diagonalization (ED) and linear spin wave theory (LSWT), we study the influence of frustration and quantum fluctuations on the magnetic ordering in the ground state of the spin-$\frac{1}{2}$ J_1-J_2 Heisenberg antiferromagnet (J_1-J_2 model) on the body-centered cubic (bcc) lattice. Contrary to the J_1-J_2 model on the square lattice, we find for the bcc lattice that frustration and quantum fluctuations do not lead to a quantum disordered phase for strong frustration. The results of both approaches (ED, LSWT) suggest a first-order transition at $J_2/J_1 \approx 0.7$ from the two-sublattice Néel phase at low J_2 to a collinear phase at large J_2.

DOI: 10.1103/PhysRevB.66.224406 PACS number(s): 75.10.Jm, 75.40.Mg

I. INTRODUCTION

The properties of the two-dimensional (2d) J_1-J_2 model have attracted a great deal of interest during the last decade (see, e.g., Refs. 1–11 and references therein). The Hamiltonian of the J_1-J_2 model is

$$H = J_1 \sum_{\langle i,j \rangle} \mathbf{S}_i \cdot \mathbf{S}_j + J_2 \sum_{[i,j]} \mathbf{S}_i \cdot \mathbf{S}_j , \tag{1}$$

where $J_1 = 1$ is the nearest neighbor and $J_2 \geqslant 0$ is the frustrating next-nearest-neighbor Heisenberg exchange. We are interested in the extreme quantum case, i.e., we consider the spin quantum number is $s = 1/2$. For the square lattice it seems to be well accepted that there is a quantum spin-liquid phase between $J_2/J_1 \approx 0.38$ and $J_2/J_1 \approx 0.60$ and that the corresponding quantum phase transitions from the Néel ordered state to the spin-liquid state at $J_2/J_1 \approx 0.38$ is of second order. The nature of the transition from the spin-liquid state to the collinear state at $J_2/J_1 \approx 0.60$ is still under discussion but there are indications that it might be of first order.[10] The Néel phase for small J_2 is characterized by an antiparallel alignment of nearest-neighbor spins with a corresponding magnetic wave vector $\mathbf{Q}_{Néel} = (\pi, \pi)$. The collinear state for large J_2 is twofold degenerated and the corresponding magnetic wave vectors are $\mathbf{Q}^1_{col} = (\pi, 0)$ and $\mathbf{Q}^2_{col} = (0, \pi)$. The two collinear states are characterized by a parallel spin orientation of nearest neighbors in vertical (horizontal) direction and an antiparallel spin orientation of nearest neighbors in horizontal (vertical) direction and therefore exhibit Néel order within the initial sublattices *A* and *B*. The properties of the spin-liquid phase are a current field of active research. Even additional quantum phase transitions at $(J_2/J_1) \approx 0.34$ and $(J_2/J_1) \approx 0.50$ are discussed.[10]

The properties of quantum spin systems strongly depend on the dimensionality. So, contrary to the 2d model, the one-dimensional J_1-J_2 model does not have a Néel ordered ground state, but exhibits a transition from a critical state to a dimer phase at $J_2/J_1 = 0.241$ (see, e.g., Refs. 12–14). Though the tendency to order is more pronounced in three-dimensional (3d) quantum spin systems than in low dimensional ones a spin-liquid phase is also observed for frustrated 3d systems like the Heisenberg antiferromagnet on the pyrochlore lattice.[15,16]

In this paper, we consider the 3d version of the J_1-J_2 model. To cover the possibility to have in a 3d model both Néel phases found for the 2d model, we need a 3d bi-bipartite lattice, i.e., a lattice consisting of two interpenetrating bipartite sublattices. The body-centered cubic (bcc) lattice consists of two interpenetrating, identical simple cubic sublattices. Each simple cubic sublattice consists of two interpenetrating, identical face-centered lattices. Therefore, the bcc lattice is a 3d bi-bipartite cubic lattice.

The classical ground state for the bcc lattice corresponds to that of the square lattice: For $J_2/J_1 < \alpha_c$ it is a usual two-sublattice Néel state, whereas for $J_2/J_1 > \alpha_c$ an antiferromagnet with four sublattices is realized. The transition point α_c depends on the coordination numbers $\alpha_c = z_1/(2z_2)$, where z_1 is the number of nearest neighbors (J_1 bonds) and z_2 of next-nearest neighbors (J_2 bonds). Consequently, we have $\alpha_c = 1/2$ for the square lattice but $\alpha_c = 2/3$ for the bcc lattice. Therefore, we define as the appropriate parameter of frustration

$$p = \frac{J_2 z_2}{J_1 z_1} \tag{2}$$

and we have $p_c^{square} = p_c^{bcc} = 1/2$.

In what follows, we use the exact diagonalization scheme and the linear spin wave theory (LSWT) to calculate the ground-state properties of the J_1-J_2 model on the bcc lattice and compare the results with the corresponding ones for the square lattice. We will present the ground-state energy, the violation of the Marshall-Peierls sign rule, the sublattice magnetizations and the spin gap of finite lattices in Sec. II. Properties of the infinite lattices will be given in Sec. III, where the results of the extrapolation of the ground-state energy, the sublattice magnetizations [from exact diagonalization (ED) data] and the corresponding results of the LSWT are shown.

TABLE I. The ten finite bcc lattices are used for exact diagonalization. $\mathbf{L}_1$, $\mathbf{L}_2$, $\mathbf{L}_3$ are the three edge vectors in upper triangle lattice form. N is the Number of sites and $\gamma=A,B,C,D,\ldots$ is an additional label corresponding to a notation used in Ref. 18 to distinguish finite lattices with identical N.

	Edge vectors		
$N\gamma$	$\mathbf{L}_1$	$\mathbf{L}_2$	$\mathbf{L}_3$
24*C*	(2,0,10)	(0,2,6)	(0,0,24)
28*D*	(2,0,10)	(0,2,6)	(0,0,28)
32*D*	(2,2,4)	(0,8,0)	(0,0,8)
32*F*	(2,0,6)	(0,4,8)	(0,0,16)
32*H*	(2,0,10)	(0,2,6)	(0,0,32)
32*J*	(4,0,4)	(0,4,4)	(0,0,8)
32*K*	(2,0,6)	(0,4,4)	(0,0,16)
36*A*	(2,0,10)	(0,2,6)	(0,0,36)
36*B*	(2,0,14)	(0,2,10)	(0,0,36)
36*C*	(2,2,4)	(0,6,6)	(0,0,12)

II. EXACT DIAGONALIZATION

A. The generation of finite bcc lattices

The generation of finite 3d lattices with periodic boundary conditions is less transparent than for 2d lattices. As has been recently pointed out by Betts and co-workers[17–19] the use of a triple of edge vectors in upper triangular lattice form[20] (utlf) leads to a systematic generation of finite 3d lattices. In this paper, we use the utlf edge vectors and follow strictly Refs. 18 and 19. Finite parallelepipeds that build up the infinite bcc lattice can be defined by three edge vectors,

$$\mathbf{L}_\alpha=\sum_{\beta=1}^{3} n_{\alpha\beta}\mathbf{a}_\beta, \tag{3}$$

where $n_{\alpha\beta}$ with $\beta=1,2,3$ are integers and $\mathbf{a}_1=(1,1,-1)$, $\mathbf{a}_2=(1,-1,1)$, $\mathbf{a}_3=(-1,1,1)$ are the basis vectors of the lattice connecting nearest neighbors. The lattice vectors connecting next-nearest neighbors are $\mathbf{b}_1=(\pm 2,0,0),\mathbf{b}_2=(\pm 0,2,0),\mathbf{b}_3=(0,0,\pm 2)$.

There are altogether ten finite bcc lattices with $N\leqslant 36$ listed in Table I, which fulfill the following three conditions: (i) Every site i of the bcc lattices should have eight nearest and six next-nearest neighbors, which means that they have the full number of nearest and next-nearest neighbors. (ii) The finite lattices should be bi-bipartite in order to avoid frustration due to boundary conditions for $p=0$ and $p\to\infty$. (Notice, that finite bcc lattices may be not bi-bipartite even though the infinite bcc lattice is.) (iii) Furthermore, they should be topologically distinct, i.e., the spin Hamiltonian (1) should exhibit different physical properties.

B. Ground-state energy

The ground-state energy gives first insight in the nature of possible zero-temperature phase transitions. In the thermodynamic limit a kink in $E_0(p)$ (respectively, a jump in the first derivative dE_0/dp) signals a first-order transition, whereas a smooth dE_0/dp is compatible with second-order transitions.

TABLE II. The ground-state energy per site of the ten considered finite bcc lattices for different values of J_2 ($J_1=1$).

	E_0/N		
$N\alpha$	$J_2=0$	$J_2=0.7$	$J_2=1.3333$
24*C*	−1.21305	−0.73883	−1.34537
28*D*	−1.20223	−0.73003	−1.32544
32*D*	−1.19572	−0.72851	−1.31225
32*F*	−1.19512	−0.72744	−1.31217
32*H*	−1.19474	−0.72708	−1.31189
32*J*	−1.19440	−0.74003	−1.31688
32*K*	−1.19408	−0.73203	−1.31423
36*A*	−1.18953	−0.72119	−1.30021
36*B*	−1.19264	−0.72180	−1.30145
36*C*	−1.19278	−0.72248	−1.30149

Furthermore, the maximum in $E_0(p)$ indicates the point of maximal frustration. The ground-state energy for the classical model consists of two straight lines $E_0^{clas}(p)=(p-1)N$ for $p\leqslant 0.5$ and $E_0^{clas}(p)=-pN$ for $p\geqslant 0.5$ with a kink (maximum) at $p=0.5$.

The quantum ground state $|\Psi_0\rangle$ is a singlet eigenstate of total spin for all J_2. In analogy to the square lattice[2] $|\Psi_0\rangle$ of finite bcc lattices with $N\mathrm{mod}8=0$ has the same translational symmetry for small and large J_2 [$\mathbf{k}_{gs}=(0,0,0)$], whereas the translational symmetry of $|\Psi_0\rangle$ for lattices with $N\mathrm{mod}4=0$ but $N\mathrm{mod}8\neq 0$ is different for small and large J_2. The change of symmetry from $\mathbf{k}_{gs}=(0,0,0)$ to $\mathbf{k}_{gs}=(\pi,\pi,\pi)$ appears slightly right from the maximum of the ground-state energy. For the quantum model, we show exact-diagonalization results of E_0/N for three different values of frustration in Table II. While $J_2=0$ and $J_2=1.3333$ correspond to zero or small frustration, $J_2=0.7$ is in the region of strong frustration.

For the sake of clearness, we present in the figures only results of selected finite lattices. To illustrate the finite-size effects in the most of the subsequent figures, we present data for the smallest (N=24) and the largest lattices we have calculated, where for $N=32,36$ we have choosen the lattices having highest symmetry. Note that the curves for lattices of identical N look very similar.

For comparison with the square lattice, we have recalculated data of Ref. 2 up to $N=6\times 6=36$. However, we think a square lattice with $N=4\times 4=16$ is comparable to a bcc lattice with $N=36$. This can be seen if one looks at the characteristic lengths $L_{3d}\propto N^{1/3}$ and $L_{2d}\propto N^{1/2}$. Further, we mention that the square lattice of $N=16$ contains five neighborhood shells, whereas some of the more dense finite bcc lattices with $N=32$ and $N=36$ contain even more.

In Fig. 1 one finds the ground-state energies of the bcc lattices 24C, 36C, and for comparison the $N=16$ and the $N=36$ square lattices. To have comparable curves, we scaled the ground-state energy of the square lattice with the factor 7/4. Figure 1 illustrates that, contrary to the 2d model, the ground-state energy of the 3d bcc lattice behaves very similarly to the classical model. As can be seen in Fig. 1 the kink in the ground-state energy is almost independent of the size

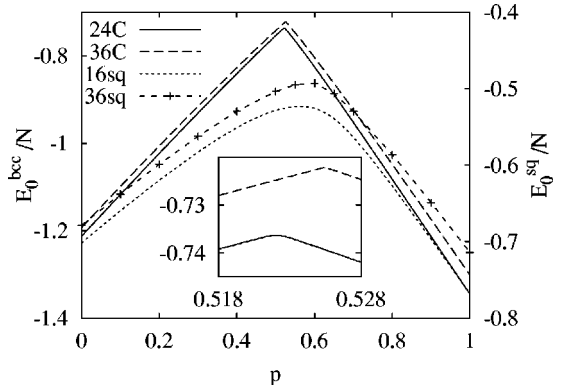

FIG. 1. Ground-state energy per site in units of J_1 for the bcc lattices 24C, 36C, and for the square lattices (scaled) with $N=16$ (16sq) and $N=36$ (36sq) versus p. The inset is an enlargement of the strongly frustrated region around $p=0.52$.

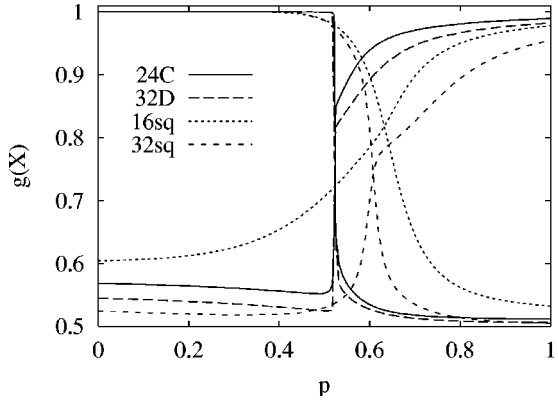

FIG. 2. The weight $g(A)$ (that is 1 for $p=0$) and $g(A_1 \cup B_1)$ (that is 1 for $p \gg 1$) of basis states $|n\rangle$ fulfilling the Marshall-Peierls sign rule for the bcc lattice 24C, 36C, and the square lattice with $N=16$ (16sq) and $N=32$ (32sq) versus p. On the bcc lattices the sign rule is completely fulfilled up to $p=0.4$ and 99.8% fulfilled at $p=0.51$.

of the bcc lattices. This can be interpreted as an indication that the kink survives in the thermodynamic limit.

C. Ground-state phase relationships

The phase relationships of the Ising basis states $|n\rangle$ in the ground state $|\Psi_0\rangle$ of the bipartite Heisenberg antiferromagnet [i.e., $J_2=0$ in (1)] follow the Marshall-Peierls sign rule.[21] This sign rule can be formulated as

$$|\Psi_0\rangle = \sum_n c_n |n\rangle \quad c_n > 0. \tag{4}$$

Here, the Ising states $|n\rangle$ are defined by

$$|n\rangle \equiv (-1)^{N/2-M(X)} |m_1\rangle \otimes |m_2\rangle \otimes \cdots \otimes |m_N\rangle, \tag{5}$$

where $|m_i\rangle$, $i=1,\ldots,N$, are the eigenstates of the site spin operator S_i^z (i.e., $m_i=\pm\frac{1}{2}$) and $M(X)=\Sigma_{i\epsilon X} m_i$. The standard Marshall-Peierls sign rule appropriate for the Néel phase at small p is obtained for $X=A$, i.e., X labels one of the two equivalent sublattices. For large values of p, we have antiferromagnetic order within the initial sublattices A and B and A and B resolve into four sublattices ($A \rightarrow A_1$, A_2 and $B \rightarrow B_1$, B_2). Then a modified sign rule holds with $X = A_1 \cup B_1$.

As pointed out in Refs. 4 and 5 and very recently in Ref. 11 the sign rule may survive some frustration but is clearly violated for the square lattice in the strongly frustrated spin-liquid region. Hence, we can use the violation of the Marshall-Peierls sign rule as an indication of the breakdown of the two-sublattice Néel state.

In Fig. 2 one finds the weight $g(X)=\Sigma_n'(c_n)^2$ of the Ising states $|n\rangle$ fulfilling the Marshall-Peierls sign rule (i.e., the sum Σ_n' is restricted to the subset of states having $c_n>0$) for two finite bcc lattices and two square lattices. For the J_1-J_2 model on the bcc lattice the rule (4) is violated almost discontinuously at that point where the ground-state energy has its maximum. This is a hint to a very drastic change of the ground state on the bcc lattice around $p=0.52$, which can be attributed to an abrupt breakdown of the two-sublattice Néel state. On the other hand, for the J_1-J_2 model on the square lattice the violation of the sign rule (4) starts smoothly and becomes significant near $p=0.4$, where the second-order transition to the spin-liquid state takes place. The modified sign rule with $g(A_1 \cup B_1)$ changes also discontinuously for the bcc lattice but smoothly for the square lattice. However, there is a violation of the modified rule also in the collinear phase, which can be attributed to the coupling between the both antiferromagnetic subsystems living on the initial sublattices A and B. Only for large $p \gg 1$, where the ground state becomes a product state of both antiferromagnetic subsystems the modified rule is rigorously fulfilled.

D. Sublattice magnetizations

Of course, the most important parameter to study Néel ordering is the sublattice magnetization. In finite systems the conventional antiferromagnetic long-range order, that is realized for small p, has to be described by the square of the sublattice magnetization of one spin component

$$m^2(\mathbf{Q}) = \left\langle \left[\frac{1}{N} \sum_{i=1}^{N} e^{i\mathbf{Q}\mathbf{R}_i} S_i^z \right]^2 \right\rangle \tag{6}$$

with $\mathbf{Q}_{N\acute{e}el}=(\pi,\pi,\pi)$ for the bcc lattice [and $\mathbf{Q}_{N\acute{e}el}=(\pi,\pi)$ for the square lattice]. For large values of p the magnetic wave vectors $\mathbf{Q}_{col}^{1,2}=(\pm\pi/2,\pm\pi/2,\pm\pi/2)$ have to be used for the bcc lattice [and $\mathbf{Q}_{col}^1=(\pi,0)$ or $\mathbf{Q}_{col}^2=(0,\pi)$ for the square lattice] to describe the collinear phase with antiferromagnetic order within the initial sublattices A and B. We denote in the following, the order parameter of the Néel phase calculated with $\mathbf{Q}_{N\acute{e}el}$ with m^2 and that of the collinear phase calculated with $\mathbf{Q}_{col}^1$ or $\mathbf{Q}_{col}^2$ with m_α^2. Notice that m_α^2 is identical for $\mathbf{Q}_{col}^1$ and $\mathbf{Q}_{col}^2$. In Table III, we give the order parameters of the ten finite bcc lattices for $J_2=0$ and $J_2=1.3333$. The behavior of m^2 and m_α^2 shown in Fig. 3 again illustrates, that the influence of the frustration on the ground-state properties is basically different for the square and bcc lattice and suggests a direct first-order transition between both Néel phases for the bcc lattice. A more detailed

TABLE III. Sublattice magnetizations m^2 and m_α^2 of the ten considered bcc lattices for different values of J_2.

$N\alpha$	m^2 $J_2=0$	m_α^2 $J_2=1.3333$
24*C*	0.09362	0.11006
28*D*	0.09057	0.10429
32*D*	0.08787	0.09958
32*F*	0.08800	0.09959
32*H*	0.08811	0.09964
32*J*	0.08819	0.09897
32*K*	0.08827	0.09933
36*A*	0.08600	0.09605
36*B*	0.08516	0.09562
36*C*	0.08509	0.09561

presentation of the transition region is given in Fig. 4. One finds that the position of the transition only slightly depends on size and symmetry of the finite lattices. Moreover, the width of transition region is getting smaller with growing N. Again, we mention that the region of transition is related to the maximum of E_0 and the significant violation of the Marshall-Peierls sign rule.

E. Spin gap

Another indication for a possible quantum disordered spin-liquid state is the spin gap, i.e., the gap Δ_{ST} between the singlet ground state and the first triplet excitation. In Néel ordered systems, we have Goldstone modes and no spin gap is observed in the thermodynamic limit. Contrary to this, quantum disorder is accompanied by the opening of a spin gap. We show the gap Δ_{ST} of two finite bcc lattices in Fig. 5. The first triplet excitation relevant for the gap belongs to the translational symmetry $\mathbf{k}_t=(\pi,\pi,\pi)$ for small p and $\mathbf{k}_t=(\pi/2,\pi/2,\pi/2)$ for large p. For comparison, we show the gap for the square lattice of $N=16$ and $N=32$ sites. Of course, the gap of a finite lattice is finite. However, in the long-range ordered Néel and collinear phases the extrapolation to the thermodynamic limit yields a vanishing gap. Obviously, there is no increase in the gap for the bcc lattices till

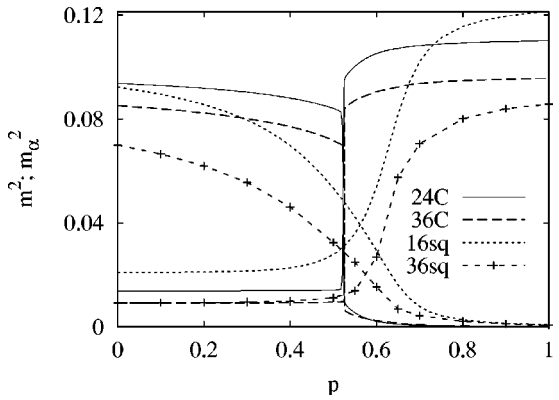

FIG. 3. Sublattice magnetizations m^2 (maximal for small p) and m_α^2 (maximal for large p) of the bcc lattices 24C, 36C, and the square lattices with $N=16$ (16sq) and $N=36$ (36sq) versus p.

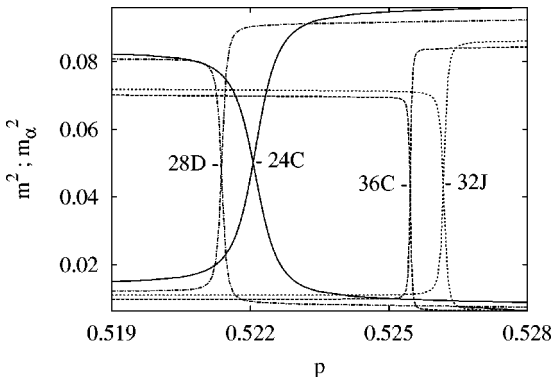

FIG. 4. Sublattice magnetizations m^2 (maximal for small p) and m_α^2 (maximal for large p) of the bcc lattice 36C, 32D, 28D, and 24C near the phase transition point $p\approx 0.52$.

about $p\approx 0.52$, where the transition from the two-sublattice Néel phase to the collinear phase takes place. In the collinear phase the relevant coupling parameter for excitations is J_2 instead of J_1 and consequently, the gap increases linearly with p. Clearly, we see that there is no special behavior of Δ_{ST} near the transition point $p\approx 0.52$. The gap for the square lattice shows a similar behavior for parameter regions where magnetic long-range order in the ground state is present, but around $p=0.5$ the behavior of Δ_{ST} is in contrast to the bcc lattice. In this region a quantum disordered gapped phase for the square lattice is expected, which is consistent with the significant increase of Δ_{ST} near $p=0.5$.

We conclude from the examination of the spin gap that there are no indications for a quantum disordered gapped phase for the bcc lattice.

III. INFINITE BCC LATTICES

A. Finite-size extrapolation

To obtain properties of the infinite bcc lattice, we extrapolate the ED data of all ten lattices listed in Table I. The finite-size extrapolation is a well elaborated approximation scheme successfully applied to many 2d quantum spin sys-

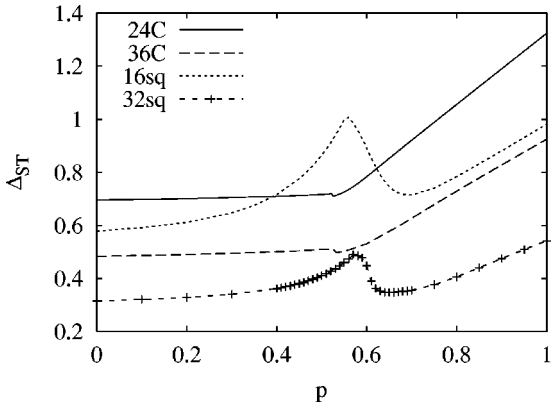

FIG. 5. Spin gap Δ_{ST} in units of J_1, i.e., the gap to the first triplet excitation for the bcc lattices 24C, 36C, and the square lattices with N=16 (16sq) and N=32 (32sq) versus p.

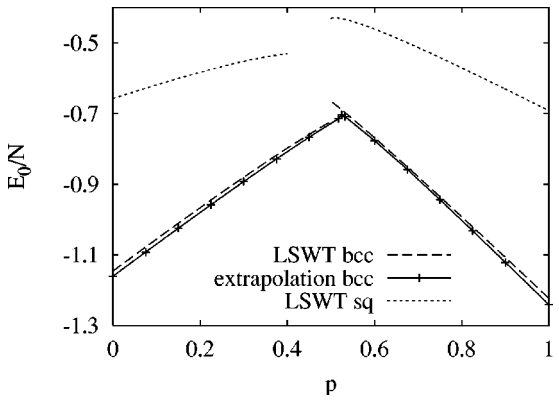

FIG. 6. LSWT data for the ground-state energies E_0 of the infinite bcc lattice (dashed line, LSWT bcc) and square lattice (dotted line, LSWT sq) as well as the extrapolated ED data for E_0 (solid line with data points) versus p.

tems like the J_1-J_2 model on the square lattice.[2] But even for 3d lattices this scheme may lead to precise data for the infinite lattice.[17–19] The corresponding scaling laws are known from literature.[22–24] The scaling equation for ground-state energy per site $\epsilon = E_0/N$ of the bcc lattice is

$$\epsilon(L) = \epsilon(\infty) + A_4 L^{-4} + \cdots \tag{7}$$

and for the order parameter

$$m^2(L) = m^2(\infty) + B_2 L^{-2} + \cdots \tag{8}$$

with $L = N^{1/3}$.

The same relation is valid for m_α^2. The results are presented in Figs. 6 and 7. The discussion of the data is given below.

B. Linear spin wave theory (LSWT)

1. LSWT for small J_2

Starting from the classical two-sublattice Néel state, we choose a two-boson representation of the Hamiltonian (1).

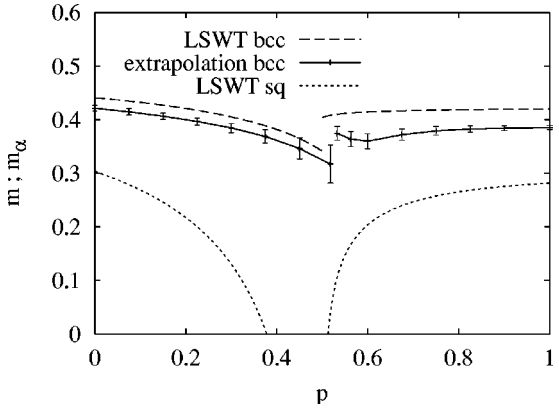

FIG. 7. LSWT data for the sublattice magnetizations m of the infinite bcc lattice (dashed line, LSWT bcc) and square lattice (dotted line, LSWT sq) as well as extrapolated ED data for $\sqrt{3m^2(\infty)}$ and $\sqrt{3m_\alpha^2(\infty)}$ (solid line with data points) versus p. The error bars indicate the standard deviation of the finite-size extrapolation.

Rewriting the spin operators of the Hamiltonian in terms of bose operators by using the usual Holstein-Primakoff transformation and taking into account only quadratic terms in the bose operators, we obtain a bosonic Hamiltonian in Fourier transformed representation

$$H = s^2 N(-8+6p) + \sum_{\mathbf{k}} \{A_{\mathbf{k}}(a_{\mathbf{k}}^+ a_{\mathbf{k}} + b_{\mathbf{k}}^+ b_{\mathbf{k}}) + B_{\mathbf{k}}(a_{\mathbf{k}} b_{-\mathbf{k}} + a_{\mathbf{k}}^+ b_{-\mathbf{k}}^+)\} \tag{9}$$

with the coefficients

$$A_{\mathbf{k}} = s[8 - 6p(1-\gamma_{2\mathbf{k}})], \tag{10}$$

$$B_{\mathbf{k}} = 8s\,\gamma_{1\mathbf{k}}. \tag{11}$$

The structure factors of nearest neighbors and next-nearest neighbors are given by

$$\gamma_{1\mathbf{k}} = \cos k_x \cos k_y \cos k_z, \tag{12}$$

$$\gamma_{2\mathbf{k}} = \frac{1}{3}(\cos 2k_x + \cos 2k_y + \cos 2k_z). \tag{13}$$

The ground-state energy per site is then

$$E_0/N = s^2(-8+6p) + \frac{1}{N}\sum_{\mathbf{k}} (\omega_{\mathbf{k}} - A_{\mathbf{k}}) \tag{14}$$

with $\omega_{\mathbf{k}} = \sqrt{A_{\mathbf{k}}^2 - B_{\mathbf{k}}^2}$. The sublattice magnetization $m = \langle S_i^z \rangle$ is

$$m = s - \frac{1}{N}\sum_{\mathbf{k}} \left(-\frac{1}{2} + \frac{A_{\mathbf{k}}}{2\omega_{\mathbf{k}}} \right). \tag{15}$$

2. LSWT for large J_2

The classical ground state of the J_1-J_2 model on the bcc lattice for large J_2 consists of two interpenetrating Néel states each living on the initial sublattices A and B. The two Néel states are energetically decoupled, i.e., the angle θ between the staggered magnetization on A and B is arbitrary for classical spins. For the quantum model, we start with arbitrary θ and use as quantization axis the local orientation of the spins in the classical ground state. The further procedure is the same as for small J_2 but the bosonic Hamiltonian now contains the angle θ. By means of the Hellmann-Feynman theorem[25] $\langle \partial H(\theta)/\partial\theta \rangle = \partial E(\theta)/\partial\theta$ it can be easily found that in the quantum model the collinear state ($\theta = 0$ or π) has lowest energy. This lifting of the continuous degeneracy of the classical ground state by quantum fluctuations (*order from disorder effect*) is also found for the square lattice.[26] For $\theta = 0$ the bosonic Hamiltonian reads

$$H = -6Nps^2 + \sum_{\mathbf{k}} \{A(a_{\mathbf{k}}^\dagger a_{\mathbf{k}} + b_{\mathbf{k}}^\dagger b_{\mathbf{k}}) + [C_{\mathbf{k}}(b_{\mathbf{k}} a_{\mathbf{k}}^+ - b_{\mathbf{k}}^+ a_{-\mathbf{k}}^+) - B_{\mathbf{k}}(a_{\mathbf{k}} a_{-\mathbf{k}} + b_{\mathbf{k}} b_{-\mathbf{k}}) + \text{H.c.}]\}, \tag{16}$$

where

$$A = 6sp, \tag{17}$$

$$B_{\mathbf{k}} = 3sp\,\gamma_{2\mathbf{k}}, \tag{18}$$

$$C_{\mathbf{k}} = 4s(\cos k_x \cos k_y \cos k_z + i \sin k_x \sin k_y \sin k_z). \tag{19}$$

Then the ground-state energy per site is

$$E_0/N = -6s^2p + \frac{1}{N}\sum_{\mathbf{k}}\left(\frac{\omega_{1\mathbf{k}}}{2} + \frac{\omega_{2\mathbf{k}}}{2} - A\right) \tag{20}$$

with the modes

$$\omega_{1\mathbf{k}} = \sqrt{A^2 - 4B_{\mathbf{k}}^2 + F_{\mathbf{k}}}; \quad \omega_{2\mathbf{k}} = \sqrt{A^2 - 4B_{\mathbf{k}}^2 - F_{\mathbf{k}}}, \tag{21}$$

and the function

$$F_{\mathbf{k}} = \{(C_{\mathbf{k}}^2 - C_{\mathbf{k}}^{*2})^2 - 8AB_{\mathbf{k}}(C_{\mathbf{k}}^2 + C_{\mathbf{k}}^{*2}) + 4C_{\mathbf{k}}C_{\mathbf{k}}^*(A^2 + 4B_{\mathbf{k}}^2)\}^{1/2}. \tag{22}$$

The sublattice magnetization is written as

$$m_\alpha = s - \frac{1}{N}\sum_{\mathbf{k}} \frac{D(\mathbf{k},\omega_{1\mathbf{k}})}{2\omega_{1\mathbf{k}}(\omega_{1\mathbf{k}}^2 - \omega_{2\mathbf{k}}^2)} - \frac{1}{N}\sum_{\mathbf{k}} \frac{D(\mathbf{k},\omega_{2\mathbf{k}})}{2\omega_{2\mathbf{k}}(\omega_{2\mathbf{k}}^2 - \omega_{1\mathbf{k}}^2)} \tag{23}$$

with

$$D(\mathbf{k},\omega_{\mathbf{k}}) = -\omega_{\mathbf{k}}^3 + A\omega_{\mathbf{k}}^2 - (4B_{\mathbf{k}}^2 - A^2)\omega_{\mathbf{k}} + A(4B_{\mathbf{k}}^2 + 2C_{\mathbf{k}}C_{\mathbf{k}}^*) - 2B_{\mathbf{k}}(C_{\mathbf{k}}^2 + C_{\mathbf{k}}^{*2}) - A^3. \tag{24}$$

The results of LSWT and the finite-size extrapolation are shown in Figs. 6 and 7. For the limits $J_2 = 0$ and $J_1 = 0$ our LSWT results are in agreement with data for the bcc and the simple cubic lattice given in.[24] Both methods yield similar results. For the ground-state energy, we have a good quantitative agreement. Being in the size of the data points, the standard deviation of extrapolated ground-state energy is not shown. For the order parameter the finite-size effects are stronger and the agreement is only qualitative. Both methods suggest a first-order transition for the spin-$\frac{1}{2}J_1$-J_2 model on the bcc lattice. The transition point obtained from the ED data is $J_2 \approx 0.7J_1$ (i.e., $p \approx 0.52$), while the LSWT becomes instable at the classical transition point.

IV. CONCLUSION

We have presented spin-wave and exact diagonalization results for the spin-$\frac{1}{2}J_1$-J_2 model on the bcc lattice and compare them with those for the square lattice. In general, we observe that the physics for the 3d quantum model is closer to classical behavior since quantum fluctuations and finite-size corrections become less important for higher coordination number and larger dimension.

We are not sure whether the increase of the magnetization m_α approaching the transition point from the right (shown in Fig. 7) is a real effect. A possible physical origin for an increase may be a stronger coupling of the Néel ordered subsystems A and B due to larger quantum fluctuations or finite-size effects that become more important in the region of strong frustration. From the data for the ground-state energy, the Marshall-Peierls sign rule, the sublattice magnetizations and the spin gap, we conclude that the increase from dimension d=2 to d=3 changes the physical properties basically. The good agreement with the spin wave results support this conclusion. Contrary to the 2d model, where the quantum fluctuations and frustration lead to a second-order transition from the two-sublattice Néel state to a disordered spin-liquid phase like, in the 3d model we find no indications for a disordered ground-state phase. The quantum J_1-J_2 model on the bcc lattice shows one transition of first order induced by strong frustration from the two-sublattice Néel state directly to the collinear state, where the transition takes place at $\alpha_c = (J_2/J_1)_c \approx 0.7$.

ACKNOWLEDGMENTS

We acknowledge support from the Deutsche Forschungsgemeinschaft (Project No. Ri 615/7-1). We also want to thank Dirk Schmalfuß for fruitful discussions.

*Electronic address: reimar.schmidt@physik.uni-magdeburg.de

[1] P. Chandra and B. Doucot, Phys. Rev. B **38**, 9335 (1988).
[2] H.J. Schulz and T.A.L. Ziman, Europhys. Lett. **18**, 355 (1992); H.J. Schulz, T.A.L. Ziman, and D. Poilblanc, J. Phys. I **6**, 675 (1996).
[3] J. Richter, Phys. Rev. B **47**, 5794 (1993).
[4] K. Retzlaff, J. Richter, and N.B. Ivanov, Z. Phys. B: Condens. Matter **93**, 21 (1993).
[5] J. Richter, N.B. Ivanov, and K. Retzlaff, Europhys. Lett. **25**, 545 (1994).
[6] R.F. Bishop, D.J.J. Farnell, and J.B. Parkinson, Phys. Rev. B **58**, 6394 (1998).
[7] R.R.P. Singh, Zheng Weihong, C.J. Hamer, and J. Oitmaa, Phys. Rev. B **60**, 7278 (1999).
[8] V.N. Kotov and O.P. Sushkov, Phys. Rev. B **61**, 11 820 (2000).
[9] L. Capriotti and S. Sorella, Phys. Rev. Lett. **84**, 3173 (2000).
[10] O.P. Sushkov, J. Oitmaa, and Zheng Weihong, Phys. Rev. B **63**, 104420 (2001).
[11] L. Capriotti, F. Becca, A. Parola, and S. Sorella, Phys. Rev. Lett. **87**, 097201 (2001).
[12] K. Okamoto and K. Nomura, Phys. Lett. A **169**, 433 (1992).
[13] S. Eggert, Phys. Rev. B **54**, R9612 (1996).
[14] Steven R. White and Ian Affleck, Phys. Rev. B **54**, 9862 (1996).
[15] B. Canals and C. Lacroix, Phys. Rev. Lett. **80**, 2933 (1998).
[16] A. Koga and N. Kawakami, Phys. Rev. B **63**, 144432 (2001).
[17] G.E. Stewart, D.D. Betts, and J.S. Flynn, J. Phys. Soc. Jpn. **66**, 3231 (1997).
[18] D.D. Betts, J. Schulenburg, G.E. Stewart, J. Richter, and J.S. Flynn, J. Phys. A **31**, 7685 (1998).
[19] J. Schulenburg, J.S. Flynn, D.D. Betts, and J. Richter, Eur. Phys. J. B **21**, 191 (2001).
[20] J.N. Lyness, T. Sorevik, and P. Keast, Math. Comput. **56**, 243

(1991).
[21] W. Marshall, Proc. R. Soc. London, Ser. A **232**, 48 (1955).
[22] H. Neuberger and T. Ziman, Phys. Rev. B **39**, 2608 (1989).
[23] P. Hasenfratz and F. Niedermayer, Z. Phys. B: Condens. Matter **92**, 91 (1993).
[24] J. Oitmaa, C.J. Hamer, and Zheng Weihong, Phys. Rev. B **50**, 3877 (1994).
[25] R.P. Feynman, Phys. Rev. **50**, 340 (1939).
[26] K. Kubo and T. Kishi, J. Phys. Soc. Jpn. **60**, 567 (1990).